BULLETIN OF THE POLISH ACADEMY OF SCIENCES
TECHNICAL SCIENCES, Vol. 71(4), 2023, Article number: e144608
DOI: 10.24425/bpasts.2023.144608

Structure and properties of magnetic composites based on amorphous Fe alloys

Bartłomiej JEŻ[1]*, Przemysław POSTAWA[1], and Marcin NABIAŁEK[2]

[1] Department of Technology and Automation, Faculty of Mechanical Engineering and Computer Science, Czestochowa University of Technology, al. Armii Krajowej 19c, 42-200 Częstochowa, Poland
[2] Department of Physics, Faculty of Production Engineering and Materials Technology, Czestochowa University of Technology, al. Armii Krajowej 19, 42-200 Częstochowa, Poland

Abstract. Materials with so-called soft magnetic properties are an important object of material engineering research due to their potential application, among others, in the construction of low-loss transformer cores. Such properties are typical for alloys with an amorphous structure and with a high content of ferromagnetic elements: Fe, Co, Ni. Difficulties related with obtaining alloys which meet satisfactory dimensions result in the search for new solutions. One of them is the production of composites based on ferromagnetic powders obtained from amorphous alloys. This paper presents results of structure research for composite materials produced in a multi-stage production process. Magnetic composites were made on the basis of a bulk amorphous $Fe_{70}B_{20}Y_5Nb_4Mo_1$ alloy produced by the injection method. On the basis of the obtained powder, two series of moldings were made: with 0.5% resin and covered with high-temperature varnish. Final composites were produced by using high temperature isostatic press. On the basis of the conducted research, it was found that the composites without resin are characterized by distinctly better magnetic properties as compared to resin-bonded composites.

Key words: bulk amorphous alloys, magnetic composites, high temperature isostatic press.

1. INTRODUCTION

Fe-matrix based amorphous alloys show good magnetic soft properties, i.e. a high value of saturation magnetization and magnetic susceptibility, and a low value of the coercive field. In particular, alloys produced in the form of a thin ribbon at high cooling rates of 10^5 K/s are characterized by excellent magnetic parameters [1–5]. Moreover, these materials have good mechanical properties [6, 7] and high corrosion resistance [8–10]. However, applicability of these alloys is significantly limited due to their dimensions – thickness of these materials does not exceed 100 μm. Therefore, for decades, one of the amorphous alloys development directions was an attempt to obtain materials of distinctly larger dimensions. This art was successful for the alloys on the Pd [11, 12] or Zr [13, 14] matrix. For alloys on the Fe matrix, attempts to produce alloys with a diameter from a few to several millimeters [15–17] have been successful, however, these alloys are characterized by a relatively low Fe content. They present good mechanical properties but do not have ferromagnetic properties [18–20]. Maximum diameters achieved for ferromagnetic alloys on the Fe matrix are about 2 mm [21, 22]. Glass transition ability of these materials is increased by the proportion of transition metals such as Mo, Nb, Cr, Y, Zr or Hf.

One of development directions for ferromagnetic amorphous alloys are composites. Fe-matrix amorphous alloys crystallize at the temperature of about 850–950 K [23]. This makes it impossible to use high-temperature composites production methods such as sintering. Therefore, amorphous powders are solidified with the use of various materials, including resins [24]. Unfortunately, such treatments significantly damage the magnetic properties. This is due to the separation of magnetic particles. For this reason, it is a good idea to cover the precompressed powder with a layer of binding substance which will provide stability to the new material without penetrating into the composite.

The aim of this work was to investigate the influence of the binder type used on the structure and magnetic properties for composites produced on the matrix of an amorphous Fe alloy.

2. MATERIALS AND METHODS

First stage in composite production was the production of a polycrystalline ingot in an arc furnace. The melting process was carried out on a water-cooled copper plate. High purity alloy components (Fe – 99.98%, Y – 99.95%, Nb – 99.95%, Mo – 99.95%, B – 99.9%) were weighed with an accuracy of 0.0001 gram. The charge was placed in a recess on the copper plate. Components were melted with a non-consumable tungsten electrode at a current in the range of 180–350 A. Solidification of the alloy was preceded by the melting of the titanium getter in order to trap the impurities remaining in the working chamber.

The process was carried out under a protective argon atmosphere after obtaining a high vacuum. The two 10-gram ingots produced were mechanically cleaned, divided into smaller

*e-mail: bartlomiej.jez@pcz.pl

Manuscript submitted 2022-09-14, revised 2023-01-05, initially accepted for publication 2023-01-05, published in August 2023.

pieces and re-cleaned in an ultrasonic cleaner. A rapidly cooled alloy was produced using the injection method. Plates with dimensions of $10 \times 5 \times 0.5$ mm were cast. A polycrystalline batch was placed in a quartz crucible and melted using eddy currents. Liquid melt was forced under argon pressure into a water-cooled copper mold. The manufacturing process was carried out in the same atmosphere as for the production of ingots. The alloy plates obtained were subjected to low-energy crushing using an agate mortar in toluene. The resulting powder was fractionated using laboratory shaker sieves. 50–100 μm fraction was selected for further research and divided into two parts. One of them was subjected to an isothermal annealing process at the temperature of 793 K for 30 minutes. Separated powder fractions were pressed inside a uniaxial hydraulic press in the air (pressing time 30 minutes, pressure 30 MPa). Four series of moldings were produced: with 0.5% chemosetting resin (Duracyl Plus, chemosetting acrylic) and without resin, and also covered with high-temperature varnish (light gasoline treated with hydrogen) with a metallic filler: fraction 50–100 μm without heat treatment and after treatment. Compacts had the following dimensions: outer diameter 10 mm, inner diameter 5 mm and thickness of 3 mm. With the use of HIP (high temperature isostatic press), magnetic composites were made from previously prepared moldings from the fraction not subjected to thermal treatment. The process was carried out with increasing argon temperature and pressure to the value of $T = 793$ K and $P = 100$ MPa. Thus, an identical thermal history for the metallic filler was obtained. Figure 1 shows a diagram of the production of test materials.

Pressing temperature was determined on the basis of the thermogram obtained from measurement by differential calorimetry (Netzsch STA 449 Jupiter). Alloy sample was heated at a rate of 10 K/s until it melted. The test was carried out under nitrogen atmosphere.

Structure of the produced materials was investigated using X-ray diffraction. A BRUKER Advanced 8 diffractometer was used. This device was equipped with a semiconductor counter and a CuKα lamp. Measurements were performed at room temperature in the range of 20–100°, angle 2O with an exposure time of 7 seconds per measurement step (0.02°).

Microstructure photos of fractures for samples in the form of wafers and composites were made using a scanning electron microscope "Supra 25 Zeiss by Detector SE" equipped with an EDS analyzer. EDS measurement results are reported with an accuracy of 0.1% at.

Surface roughness was determined using a KEYENCE optical microscope at 1000× magnification.

Static magnetic hysteresis loops were measured using a LakeShore VSM 7307 vibration sample magnetometer. Measurements were performed in the range of external magnetic field strengths up to 2 T at room temperature.

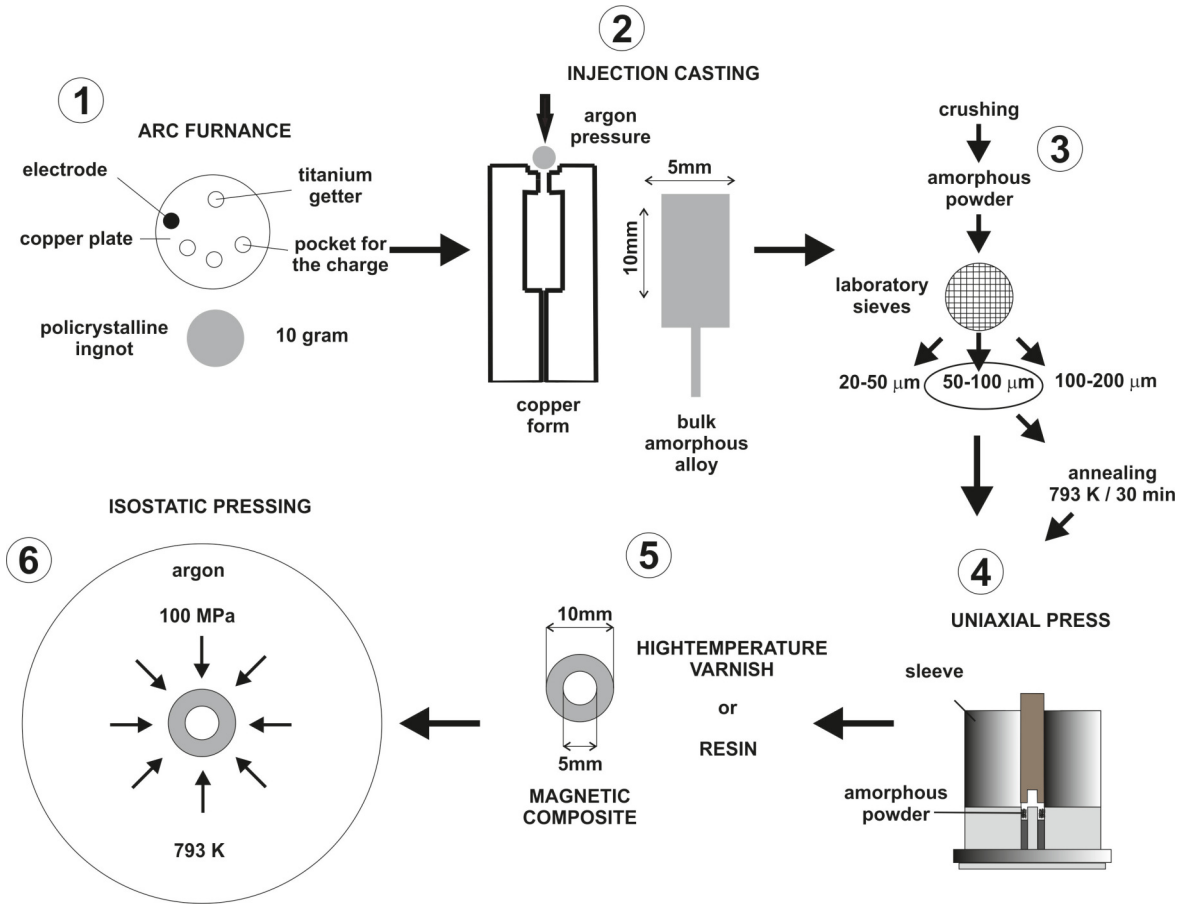

Fig. 1. Production diagram of composites based on amorphous alloys

3. RESULTS

The $Fe_{70}B_{20}Y_5Nb_4Mo_1$ alloy in the solidified state was tested for thermal stability. A thermogram developed for the tested alloy along with the determined characteristic temperatures is shown in Fig. 2.

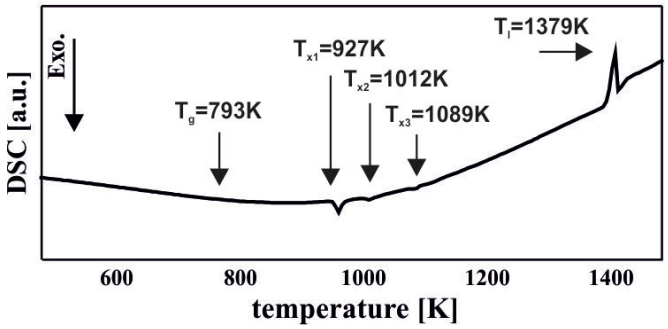

Fig. 2. DSC curve for $Fe_{70}B_{20}Y_5Nb_4Mo_1$ alloys

Based on the analysis of the DSC curve, the glass transition temperature, crystallization beginning point, secondary crystallization temperature and the melt temperature were all determined. Crystallization temperature of the alloy is typical for amorphous materials with a high content of Fe and B [23]. Temperature at which samples were subjected to isostatic pressing was set in the T_g range when the material was so-called semi-plastic. Then it became possible to solidify particles under high pressure, such as Spark plasma sintering [25, 26]. Figure 3 shows the X-ray diffraction images for the tested samples.

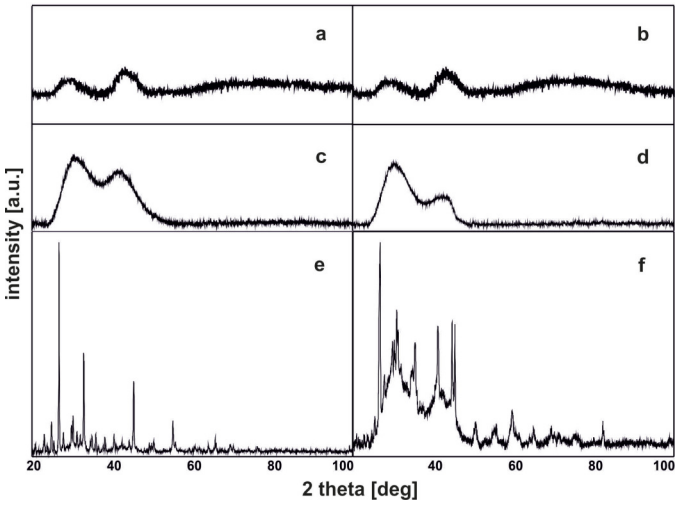

Fig. 3. X-ray diffraction patterns for $Fe_{70}B_{20}Y_5Nb_4Mo_1$ alloy: a) powder, b) powder after annealing 793 K/30 min, c) composite with 0.5% resin (annealing powder), d) composite with 0.5% resin after HIP process, e) composite covered high temperature varnish (annealing powder), f) composite covered high temperature varnish after HIP process

In Figs. 3a and 3b, there are no visible narrow peaks indicating the presence of crystalline phases. Only a wide diffuse maximum is observed in the range of 40–50° angle 2O, typical for amorphous materials. The isothermal annealing process did not affect the structure of the tested alloy. Figures 3c and 3d are similar to each other and show the X-ray diffraction patterns for the resin composite after pressing in a uniaxial and isostatic press. Measurements (Fig. 3d) were made at the temperature of 793 K so as not to cause crystallization of the amorphous filler. It can be concluded that the amorphous structure of the alloy was preserved. X-ray tests (Fig. 3e and 3f) are performed for a powdered alloy covered only with high-temperature varnish. An X-ray image obtained for uniaxial pressing reflects the structure of the applied high-temperature varnish. After the isostatic pressing process at a temperature close to T_g, the continuity lines of the applied varnish film were broken. Therefore, in addition to clear peaks from the crystalline phases, a wide diffuse increase in intensity is observed, typical of materials characterized by short-range interactions. Figure 4 presents SEM images taken for the $Fe_{70}B_{20}Y_5Nb_4Mo_1$ alloy sample.

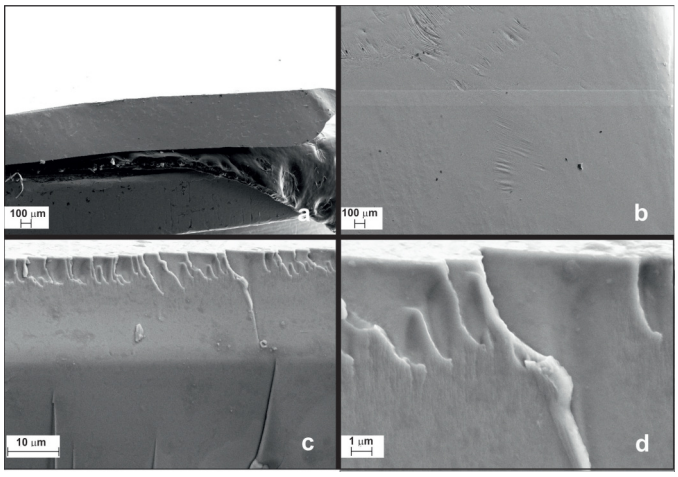

Fig. 4. SEM image for $Fe_{70}B_{20}Y_5Nb_4Mo_1$ alloy: a) general view, b) plate surface, c) plate cross-section, d) enlargement of the plate cross-section

Fractures obtained for the sample in solid state are smooth, there are no perpendicular walls, which would indicate the presence of areas related to the crystallization of the alloy in the alloy volume. However, in certain places there are other microstructures typical for amorphous materials. We can distinguish the vein microstructure and typical breakages of the material near its surface, which can be compared to a poorly developed scale microstructure. Using SEM tests, one can indirectly conclude about the solidification process of the alloy. In this case, solidification of the material proceeded with similar dynamics over the entire sample volume. However, presence of residual amounts of veins produced in the middle of the fracture indicates that the solidification process proceeded from the surface to the interior. Observed lines prove that structural relaxation processes began to take place in the volume of the material, resulting in a change of ductile amorphous alloys plasticity. In this case, brittleness of the material should be expected to increase. Additional areas, for example unmixed alloy components, cannot be distinguished in the presented cross-section. Such breakthrough proves that alloy components were

well mixed through appropriately selected production parameters. Each structure is related to the degree of its relaxation. It is evident that during the decohesion process, the force applied acts unevenly from the surface of material. In order to obtain appropriate particles of the metallic filler (appropriate particles are understood as such gradations of the alloy particles for which, with the assumed parameters of the pressing process, a coherent material is obtained), a series of attempts was made to produce rings. The best results were obtained for fraction 50–100 μm and this sample was selected for further research. However, the meshed metallic particles did not provide adequate structural stability to the compact, which caused them to crumble when a minimum force was applied to them. Metallic particles of Fe-B alloys with the addition of rare earth elements are very often caked with metallic dust. Such a phenomenon is observed when a crystalline phase from the $Y_2Fe_{14}B$ family, which is a magnetically hard phase, is formed during grinding in the volume of the alloy. In the low-energy grinding process, not all particles are uniform, and they may break (Fig. 5d), which, with further preparation, may result in the presence of particles outside the established range. Figure 5 shows the photos for the composite made of resin and metallic filler.

Photo 5a shows the composite surface, confirming its cohesion for such small proportion of the binder. Fracture obtained by decohesion shows uneven distribution of the resin within the composite. Most likely, the resin in these areas does not perform as a binder and the composite has lower strength. After careful analysis of several breakthroughs, it can be concluded that the case described above is a special one and it comes as a consequence of a poorly performed pressing process. For a series of samples that were made with a constant feed of the press mandrel with a so-called 30 minute hold, the resin was evenly distributed in the composite, as shown in Fig. 5b. Figure 6 shows the results of the chemical composition analysis performed with a system using secondary electron dispersion.

As shown by the results presented in the tables in Fig. 6, white areas correspond to the resin used for bonding metallic particles. EDS tests for the alloy particles revealed that there is

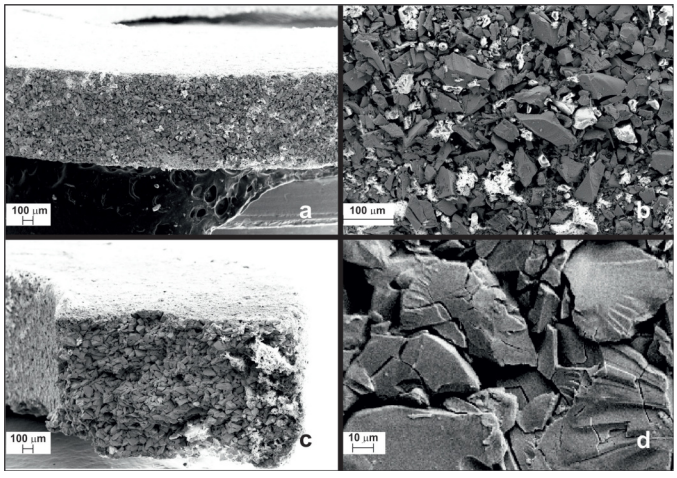

Fig. 5. SEM image for composite with 0.5% resin: a) general view, b) composite surface, c) composite cross-section, d) enlargement of the composite cross-section

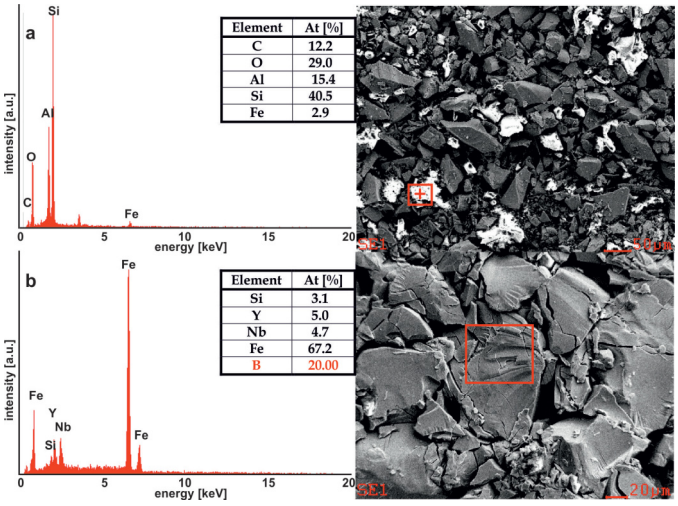

Fig. 6. EDS analysis for composite with 0.5% resin: a) resin-rich area, b) resin-free area

a small amount of silicon in its volume. Presence of this element in the alloy is related to the cycle of producing rapidly-cooled alloys on its own using the injection method. During the eddy current melting of the ingot piece, the silicon quartz crucible passes into the liquid alloy, the temperature of which is about 2300K. Photos of samples in the form of toroids without the use of resin and only covered with a layer of high-temperature varnish are shown in Fig. 7.

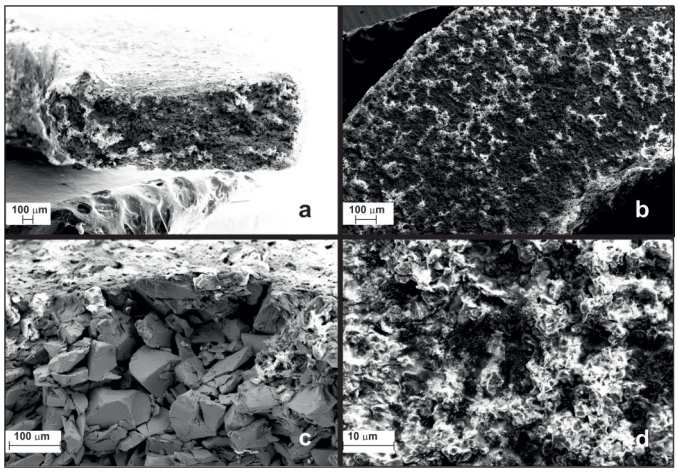

Fig. 7. image for composite covered high temperature varnish: a) general view, b) composite surface, c) composite cross-section, d) enlargement of the composite surface

Cohesion of the toroid and increased strength was obtained after applying high-temperature varnish. It only penetrates the gap between metallic particles (Fig. 7c). Composition analysis for toroidal samples covered with high-temperature varnish is presented in Fig. 8.

In accordance with the assumptions, only the high-temperature varnish (Fig. 8a) is on the surface of the sample, and directly below its surface there are intermeshing metallic filler grains with a chemical composition close to the set one (Si ad-

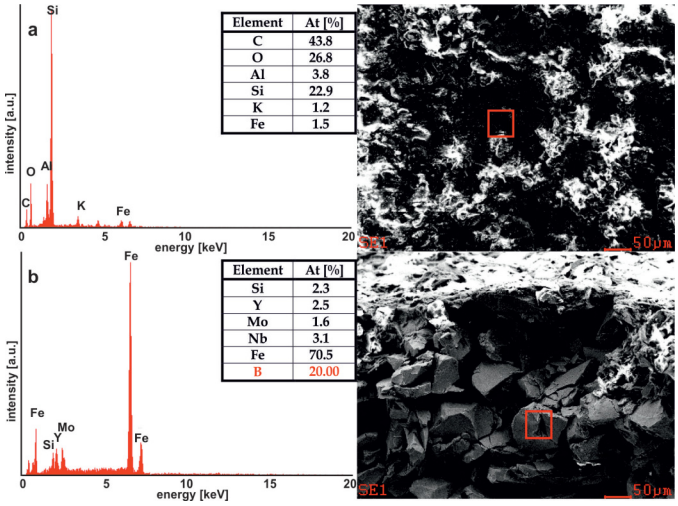

Fig. 8. EDS analysis for composite covered high temperature varnish: a) composite surface, b) composite cross-section

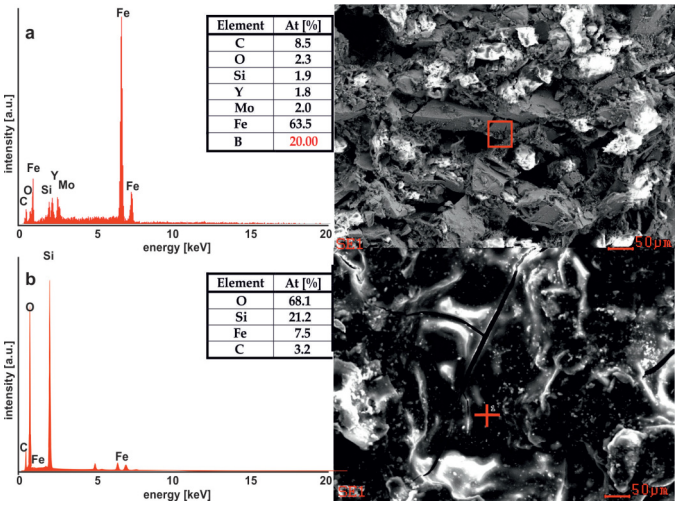

Fig. 10. EDS analysis for composite covered high temperature varnish after HIP process: a) composite cross-section, b) composite surface

dition coming from the production process). A similar analysis was performed after the high-temperature isostatic pressing process at the glass transition temperature T_g. Figure 9 shows SEM images for the tested sample, and EDS analysis is shown in Fig. 10.

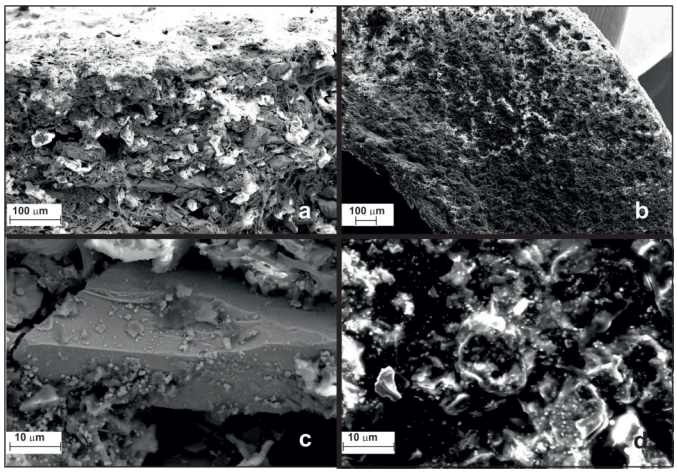

Fig. 9. SEM image for composite covered high temperature varnish after HIP process: a) general view, b) composite surface, c) composite cross-section, d) enlargement of the composite surface

External image of the sample after the isostatic pressing process is similar to the sample before the process. The varnish layer is undamaged and still fulfills its function. After the HIP process, it was noticed that the volume of the metallic toroid had decreased.

This means that the effect of obtaining a higher packing of metallic particles has been achieved. After the sample was broken, SEM analysis was performed, which shows that the HIP has no effect on the movement of the varnish into the sample (Fig. 9b). In addition, the varnish does not adhere well to metallic particles in all places (Fig. 9c). Results of EDS analysis (Fig. 10) for the surface after HIP is the same as before the process. Varnish surface is characterized by lower surface development as compared to the resin samples. Roughness measurements are shown in Figs. 11–13.

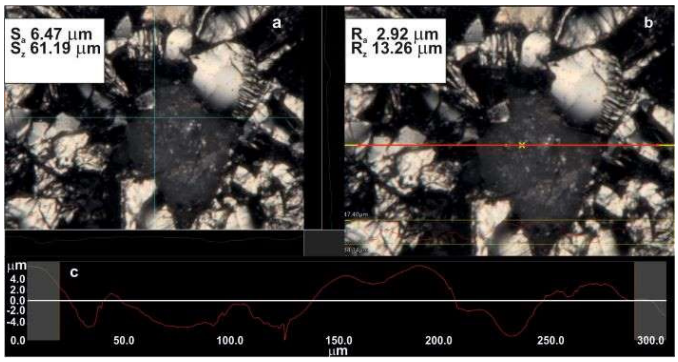

Fig. 11. Roughness for composite with 0.5% resin: a) profile for a surface, b), c) profile for a horizontal line

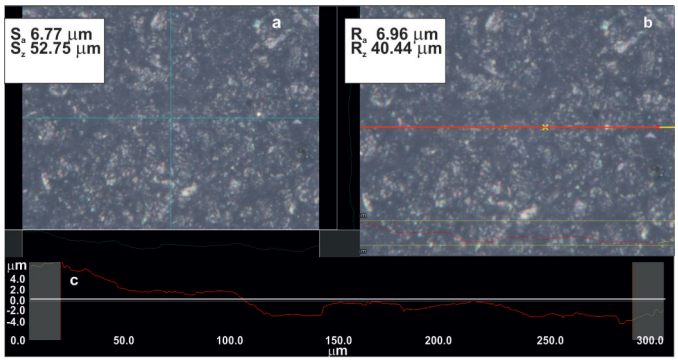

Fig. 12. Roughness for composite covered high temperature varnish: a) profile for a surface, b), c) profile for a horizontal line

Roughness of the samples is related to the form of the material – particles of non-uniformly shaped metallic filler – and to the manufacturing process: under the applied pressure and

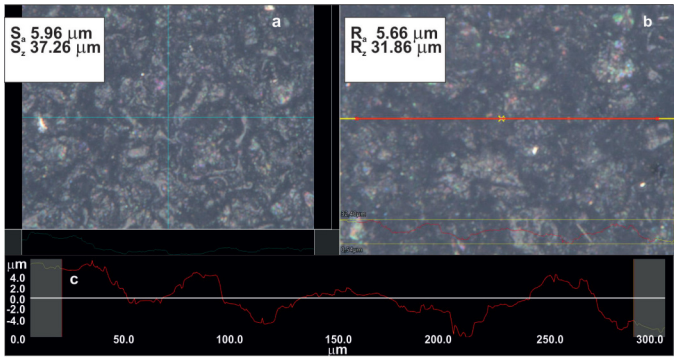

Fig. 13. Roughness for composite covered high temperature varnish after HIP process: a) profile for a surface, b), c) profile for a horizontal line. S_a – arithmetic mean deviation of the height of surface unevenness from the reference plane; S_z – maximum height of the 3D profile; R_a – arithmetic mean deviation of the profile from the mean line; R_z – greatest height of the roughness profile

specificity of the material, when the samples were withdrawn, a small part of the material remained on the mold walls. As shown by the results obtained from the roughness measurements, the greater maximum roughness height R_z and the higher value of the R_a parameter occurred for the samples covered with varnish (Fig. 11b, 11c, 12b, 12c, 13b, 13c). However, values measured for the surfaces indicate lower roughness for the painted samples. Varnish allows for distinctly better filling of the voids between the metallic filler particles, as indicated by the lower values of the S_a and S_z parameters.

Moreover, after the HIP process, these values decreased. Roughness profile for the sample after the HIP process (Fig. 13c) looks different than for the other samples. There is a clear periodicity related to the size of the filler particles (profile shows maxima at distances of about 50–60 µm). It should be concluded that some of the varnish has evaporated or has been moved inside the sample, but only at a short distance, as shown by the SEM images in Fig. 9. Filler particles on the surface are therefore covered with a layer of thinner varnish. This explains appearance of a maximum typical for amorphous materials on the diffraction pattern measured for this sample (Fig. 3f).

The aim of this experiment was to create magnetic toroids with soft magnetic properties suitable for application. Analysis of the basic properties was performed on the basis of static magnetic hysteresis loops (Fig. 14). All static magnetic hysteresis loops shown in Fig. 14 are typical ferromagnetic materials with soft magnetic properties. However, it is evident that the values of coercive field and saturation magnetization strongly depend on the form of tested samples. The resulting magnetic properties are shown in Table 1.

The lowest value of coercive field was obtained for alloy sample after solidification. As the results show, the fraction of 50–100 µm showed better properties and it was used for the production of composites. Unfortunately, introducing 0.5% of resin increased the value of the coercive field more than 20 times. Rapid increase in the coercive force field also occurred for the sample covered with high-temperature varnish. Increasing the packing of metallic particles after the HIP process resulted in a significant reduction in the HC value. However, this value in terms of soft magnetic materials is large. Similar relationships as for HC were also observed for the value of saturation magnetization.

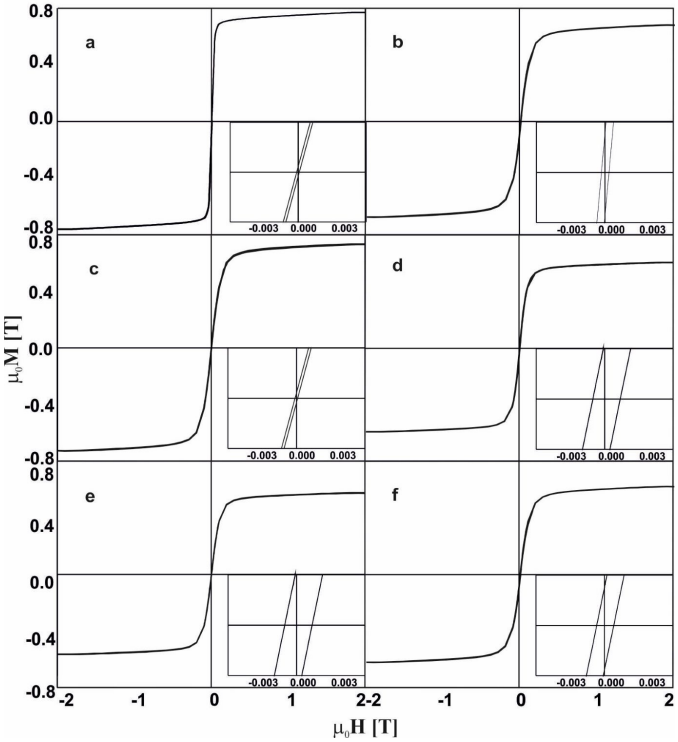

Fig. 14. Static magnetic hysteresis loops for: a) alloy after solidification, b) amorphous powder 50–100 µm, c) amorphous powder 50–100 µm after annealing 793 K/30 min, d) composite with 0.5% resin (annealing powder), e) composite covered high temperature varnish (annealing powder), f) composite covered high temperature varnish after HIP process

Table 1
Magnetic properties of testing materials

$Fe_{70}Y_5Nb_4Mo_1B_{20}$	Magnetic properties	
	H_c [A/m]	M_s [T]
ASQ	28	0.87
50–100 µm	82	0.79
50–100 µm annealing	38	0.83
composite with resin	810	0.6
composite with varnish	700	0.6
composite with varnish (HIP)	360	0.63

4. CONCLUSIONS

The aim of the study was to obtain magnetically soft toroids with a coercive field value comparable to that obtained for the fraction from which toroids were produced. According to the assumptions that in the T_g range, alloy exhibits a semi-plastic

state, it will be possible to pack metallic particles to a maximum extent and even to partially assemble them. As indicated by the results of SEM studies, use of isostatic pressing at high temperature increased the packing of metallic particles. Careful observation of SEM did not confirm that any metallic particles fused together under the influence of temperature T_g and pressure in the 30-minute process. It was found that even the residual amount of resin (0.5%), ensuring the relative consistency of the material, was the reason for drastic increase in HC and a sharp decrease in MS. Exactly the same relationship was observed for the varnished toroid. Carrying out the HIP process for the toroid resulted in a two-fold decrease in the value of the coercive field in relation to samples with resin and with varnish made of annealed metallic particles with a fraction of 50–100 μm. It was clearly indicated that the temperature of isostatic heating near T_g temperature has the effect of improving the soft magnetic properties.

REFERENCES

[1] Y. Han *et al.*, "New Fe-based soft magnetic amorphous alloys with high saturation magnetization and good corrosion resistance for dust core application," *Intermetallics*, vol. 76, pp. 18–25, 206, doi: 10.1016/j.intermet.2016.05.011.

[2] C. Dong *et al.*, "Soft magnetic properties of $Fe_{82\text{-}83}B_{14\text{-}15}Si_2C_{0.5\text{-}1}$ amorphous alloys with high saturation magnetization above 1.7 T," *J. Non-Cryst. Solids*, vol. 500, pp. 173–180, 2018, doi: 10.1016/j.jnoncrysol.2018.07.072.

[3] F. Wang *et al.*, "Excellent soft magnetic Fe-Co-B-based amorphous alloys with extremely high saturation magnetization above 1.85 T and low coercivity below 3 A/m," *J. Alloy. Compd.*, vol. 711, pp. 132–142, 2017, doi: 10.1016/j.jallcom.2017.03.341.

[4] J. Wang, Z.W. Liu, Z.G. Zheng, H.Y. Yu, G.P. Tang, and D.C. Zeng, "Efect of rare earth additions on microstructure, thermal stability and crystallization behavior of melt spun $Fe_{80.65}Cu_{1.35}Si_2B_{14}RE_2$ (RE=Y, Gd, Tb and Dy) soft magnetic alloys," *Mater. Lett.*, vol. 159, pp. 76–79, 2015, doi: 10.1016/j.matlet.2015.06.078.

[5] Y. Han *et al.*, "Fe-based soft magnetic amorphous alloys with high saturation magnetization above 1.5 T and high corrosion resistance," *Intermetallics*, vol. 54, pp. 169–175, 2014, doi: 10.1016/j.intermet.2014.06.006.

[6] Y. Han *et al.*, "Softening and good ductility for nanocrystal-dispersed amorphous FeCoB alloys with high saturation magnetization above 1.7 T," *J. Alloy. Compd.*, vol. 657, pp. 237–245, 2016, doi: 10.1016/j.jallcom.2015.10.066.

[7] S. Kwon, S. Kim, and H. Choi-Yim, "Effects of Fe Substitution for Co on the Thermal, Magnetic, and Mechanical Properties of the Co-Fe-B-Si-Mo alloy system," *Korean Phys. Soc.*, vol. 72, no. 1, pp. 171–176, 2018, doi: 10.3938/jkps.72.171.

[8] D.D. Liang *et al.*, "Sliding tribocorrosion behavior of Fe-based bulk metallic glass under corrosive environments," *J. Non-Cryst. Solids*, vol. 510, pp. 62–70, 2019, doi: 10.1016/j.jnoncrysol.2018.12.024.

[9] S. Wang, Y. Li, X. Wang, S. Yamaura, and W. Zhang, "Glass-forming ability, thermal properties, and corrosion resistance of Fe-based (Fe, Ni, Mo, Cr)-P-C-B metallic glasses," *J. Non-Cryst. Solids*, vol. 476, pp. 75–80, 2017, doi: 10.1016/j.jnoncrysol.2017.09.028.

[10] N. Hua *et al.*, "Corrosive wear behaviors and mechanisms of a biocompatible Fe-based bulk metallic glass," *J. Non-Cryst. Solids*, vol. 542, p. 120088, 2020, doi: 10.1016/j.jnoncrysol.2020.120088.

[11] H.S. Chen and D. Turnbull, "Stability and structure of palladium-silicon based alloy glasses," *Acta Metallurgica*, vol. 17, pp. 1021–1031, 1969, doi: 10.1016/0001-6160(69)90048-0.

[12] H.S. Chen, "Thermodynamic considerations on the formation and stability of metallic glasses," *Acta Metallurgica*, vol. 22, pp. 1505–1511, 1974, doi: 10.1016/0001-6160(74)90112-6.

[13] X.M. Qin, J. Tan, C.J. Li, X.C. Wang, Y.H. Jiang, and R. Zhou, "On the formation, mechanical properties and crystallization behaviors of a Zr56Co24Al20 bulk metallic glass," *J. Alloy. Compd.*, vol. 647, pp. 204–208, 2015, doi: 10.1016/j.jallcom.2015.04.241.

[14] J. Tan *et al.*, "Formation of Zr-Co-Al bulk metallic glasses with high strength and large plasticity," *Intermetallics*, vol. 31, pp. 282–286, 2012, doi: 10.1016/j.intermet.2012.08.003.

[15] S.F. Guo, K.C. Chan, S.H. Xie, P. Yu, Y.J. Huang, and H.J. Zhang, "Novel centimeter-sized Fe-based bulk metallic glass with high corrosion resistance in simulated acid rain and seawater," *J. Non-Cryst. Solids*, vol. 369, pp. 29–33, 2013, doi: 10.1016/j.jnoncrysol.2013.02.026.

[16] J. Pan, Q. Chen, N. Li, and L. Liu, "Formation of centimeter Fe-based bulk metallic glasses in low vacuum environment," *J. Alloy. Compd.*, vol. 463, pp. 246–249, 2008, doi: 10.1016/j.jallcom.2007.09.124.

[17] A. Inoue, F.L. Kong, Q.K. Man, B.L. Shen, R.W. Li, and F. Al-Marzouki, "Development and applications of Fe- and Co-based bulk glassy alloys and their prospects," *J. Alloy. Compd.*, vol. 615, pp. S2–S8, 2014, doi: 10.1016/j.jallcom.2013.11.122.

[18] S. Hasani, P. Rezaei-Shahreza, A.Seifoddini, and A. Hakimi, "Enhanced glass-forming ability, mechanical, and magnetic properties of $Fe_{41}Co_7Cr_{15}Mo_{14}Y_2C_{15}B_6$ bulk metallic glass with minor addition of Cu," *J. Non-Cryst. Solids*, vol. 497, pp. 40–47, 2018, doi: 10.1016/j.jnoncrysol.2018.05.021.

[19] P. Rezaei-Shahreza, A. Seifoddini, and S. Hasani, "Non-isothermal kinetic analysis of nano-crystallization process in (Fe41Co7Cr15Mo14Y2C15)94B6 amorphous alloy," *Thermochim. Acta*, vol. 652, pp. 119–125, 2017, doi: 10.1016/j.tca.2017. 03.017.

[20] P. Rezaei-Shahreza, A. Seifoddini, and S. Hasani, "Thermal stability and crystallization process in a Fe-based bulk amorphous alloy: The kinetic analysis," *J. Non-Cryst. Solids*, vol. 471, pp. 286–294, 2017, doi: 10.1016/j.jnoncrysol.2017.05.044.

[21] Y. Geng *et al.*, "Magnetic properties and a structuremodel for high Fe-content Fe–B–Si–Zr bulk glassy alloys," *J. Non-Cryst. Solids*, vol. 450, pp. 1–5, 2016, doi: 10.1016/j.jnoncrysol.2016.07.032.

[22] J. Zhou, W. Yang, C. Yuan, B. Sun, and B. Shen, "Ductile FeNi-based bulk metallic glasses with high strength and excellent soft magnetic properties," *J. Alloy. Compd.*, vol. 742, pp. 318–324, 2018, doi: 10.1016/j.jallcom.2018.01.317.

[23] M. Nabiałek, "Reduced glass-transition temperature versus glass-forming ability in FeCoB-based amorphous alloys," *Arch. Metall. Mater.*, vol. 61, no 4, pp. 1957–1962, 2016, doi: 10.1515/amm-2016-0315.

[24] B. Jeż, K. Jeż, and M. Nabiałek, "Magnetic Properties of Composites Based on Amorphous Iron Alloys Produced with the Use of a Non-Magnetic Binder and Covered with High Temperature Varnish," *IOP Conf. Series: Materials Science and Engineering*, vol. 877, p. 012027, 2020, doi: 10.1088/1757-899X/877/1/012027.

[25] A. Sahu, R.S. Maurya, S. Dinda, and T. Laha, "Phase Evolution-Dependent Nanomechanical Properties of $Al_{86}Ni_8Y_6$ and $Al_{86}Ni_6Y_{4.5}Co_2La_{1.5}$ Spark Plasma-Sintered Bulk Amorphous Composites," *Metall. Mater. Trans. A*, vol. 51, pp. 5110–5119, 2020, doi: 10.1007/s11661-020-05916-9.

[26] H. Kasturi, T. Paul, S. Biswas, S.H. Alavi, and S.P. Harimkar, "Sliding Wear Behavior of Spark-Plasma-Sintered Fe-Based Amorphous Alloy Coatings on Cu-Ni Alloy," *J. Mater. Eng. Perform.*, vol. 27, pp. 3629–3635, 2018, doi: 10.1007/s11665-018-3470-z.